Molecular Mechanism of the Zn^{2+}-Induced Folding of the Distal CCHC Finger Motif of the HIV-1 Nucleocapsid Protein

Elisa Bombarda,*† Ernst Grell,† Bernard P. Roques,‡ and Yves Mély*

*UMR 7175, Centre National de la Recherche Scientifique, Université Louis Pasteur, Faculté de Pharmacie, Illkirch, France; †Max-Planck-Institut für Biophysik, Frankfurt, Germany; and ‡Laboratoire de Pharmacochimie Moléculaire et Structurale, INSERM U266, Paris, France

ABSTRACT HIV-1 nucleocapsid protein, NCp7, contains two highly conserved CCHC zinc fingers. Binding of Zn^{2+} drives NCp7 from an unfolded to a highly folded structure that is critical for its functions. Using the intrinsic fluorescence of Trp^{37}, we investigated, by the stopped-flow technique, the folding of NCp7 distal finger through the pH dependence of its Zn^{2+} association and dissociation kinetics. Zn^{2+} binding was found to involve four different paths associated with the four deprotonated states of the finger. Each binding path involves the rapid formation of an intermediate complex that is subsequently rearranged and stabilized in a rate-limiting step. The equilibrium and kinetic rate constants of the full Zn^{2+}-binding process have been determined. At neutral pH, the preferential pathway for the Zn^{2+}-driven folding implies Zn^{2+} binding to the deprotonated Cys^{36} and His^{44} residues, in the bidentate state of the finger. The resulting intermediate is then converted with a rate constant of 500 s^{-1} into a more suitably folded form, probably through a rearrangement of the peptide backbone around Zn^{2+} to optimize the binding geometry. This form then rapidly leads to the final native complex, through deprotonation of Cys^{39} and Cys^{49} residues and intramolecular substitution of coordinated water molecules. Zn^{2+} dissociation is also characterized by a multistep process and occurs fastest via the deprotonated Zn^{2+}-bound bidentate state with a rate constant of 3 s^{-1}. Due to their critical role in folding, the intermediates identified for the first time in this study may constitute potential targets for HIV therapy.

INTRODUCTION

A large number of protein domains folds stably by binding a metal ion (1). This is notably the case of the zinc fingers since their proper folding depends solely on the binding of Zn^{2+} and can be studied independently of the bulk protein (1,2). This structural role of Zn^{2+} is illustrated by the HIV-1 nucleocapsid protein, NCp7, which is a small basic protein with two highly conserved CCHC zinc fingers (1,3,4). The two fingers of NCp7 bind Zn^{2+} strongly and this results in a conformational change from an unfolded to a highly folded structure (5–9). Besides its histone-like activity (10,11), NCp7 plays a role in several key steps of the viral life cycle through interactions with nucleic acids and viral proteins (4,12–15). The Zn^{2+}-promoted folding of the fingers is critical for most NCp7 functions. Indeed, Zn^{2+} ejecting agents that disrupt the zinc fingers (16,17) and amino-acid mutations (18–21) that prevent or affect Zn^{2+} binding, lead to noninfectious viruses. Disrupted or mutated NCp7 sequences fail to recognize and package the genomic RNA into new virus particles. Zn^{2+} coordination is also required for NCp7 nucleic acid chaperone activity, which assists the rearrangement of nucleic acid molecules into their most stable conformation notably during reverse transcription (15,22–27). The critical role of NCp7 zinc fingers in HIV-1 replication, together with their highly conserved sequence, makes these domains attractive targets for the development of antiviral drugs (16,28,29).

Due to their Zn^{2+}-triggered folding, the zinc fingers of NCp7 are suitable tools to investigate protein folding. In a previous study, we have investigated at equilibrium the Zn^{2+} coordination to the (35–50)NCp7 peptide (Fig. 1), representing the C-terminal finger of NCp7 (9). The four Zn^{2+}-coordinating residues (Cys^{36}, Cys^{39}, His^{44}, Cys^{49}) were found to deprotonate nearly sequentially, suggesting a stepwise binding of Zn^{2+} to these residues. Since the complexity of the binding mechanism increases with the number of Zn^{2+}-coordinating residues, we investigated first the binding kinetics of two selected point mutated peptides where one of the coordinating residues was mutated into a noncoordinating one (30). The kinetics of Zn^{2+} binding and dissociation to these point-mutated peptides indicate a multistep process involving three Zn^{2+} binding paths due to three deprotonated states of the coordinating motif (30). In both point-mutated peptides, the Zn^{2+} binding process is initiated by the deprotonation of Cys^{36} residue while the final complex is reached by subsequent stepwise ligand deprotonation and intramolecular substitution of coordinated water molecules. Moreover, the binding rate constants of the various deprotonated states of the point-mutated peptides suggested that conformational constraints are required to achieve proper metal coordination during folding. The mechanistic analysis of the point-mutated peptides thus provided a good starting point for the interpretation of the more complex binding behavior of the native peptide.

In this work, we investigate the dynamics of Zn^{2+} association and dissociation to (35–50)NCp7 at different pH values by the stopped-flow technique under anaerobic conditions.

Submitted November 17, 2006, and accepted for publication February 22, 2007.

Address reprint requests to E. Bombarda, E-mail: elisa.bombarda@uni-bayreuth.de; or Y. Mély, E-mail: mely@pharma.u-strasbg.fr.

Editor: Heinrich Roder.

0006-3495/07/07/208/10 $2.00

doi: 10.1529/biophysj.106.101378

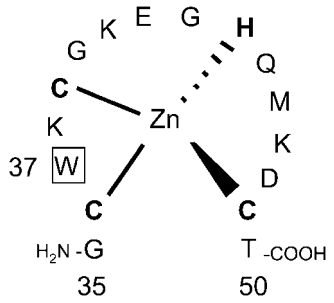

FIGURE 1 Amino-acid sequence of (35–50)NCp7. Trp^{37} is boxed.

The binding of Zn^{2+} is monitored through the Trp^{37} intrinsic fluorescence, which constitutes a sensitive reporter for the folding of NCp7 distal finger (9,30,31). Binding of Zn^{2+} to (35–50)NCp7 is characterized by two kinetic phases involving the rapid formation of intermediates that are subsequently rearranged in a rate-limiting step to lead to the constrained final complex. Our data allow us to develop a general reaction scheme and to propose the preferred pathway for Zn^{2+} binding and associated folding at neutral pH.

MATERIALS AND METHODS

Materials

The (35–50)NCp7 peptide was synthesized in its apo-form by solid-phase synthesis and purified by HPLC as previously described (32). Buffers were chosen to cover the following pH ranges: *n,n′*-diethyl-*n,n′*-bis-(sulfopropyl)-ethylenediamine (DESPEN) for pH 4.7–5.6, 2-(*n*-morpholino)-ethanesulfonic acid (MES) for pH 5.6–6.8, 4-(2-hydroxyethyl)-piperazine-1-ethanesulfonic acid (HEPES) for pH 6.8–8.5. To minimize interactions between electrolyte anions and Zn^{2+}, $NaClO_4$ was used to fix the ionic strength at 0.15 M. The Zn^{2+} solutions were prepared with $Zn(ClO_4)_2$ and degassed before use. Experimental conditions were such that hydrolysis of Zn^{2+} was avoided. The peptides were dissolved in degassed buffer and poured immediately into quartz cells (Hellma, Muellheim/Baden, Germany) specifically conceived to maintain an inert argon atmosphere. The −SH content of the free peptides during the experiments was reduced by less than 15% as checked by titration with 5,5′-dithiobis(2-nitrobenzoic acid) (33).

Absorption and fluorescence spectroscopy

Peptide concentration was determined on a HP8450A diode array (Hewlett-Packard, Palo Alto, CA) absorption spectrophotometer, using a molar extinction coefficient of 5700 M^{-1} cm^{-1} at 280 nm. Fluorescence spectra were recorded at 20 ± 0.5°C with a thermostated Fluorolog 212 (Spex CertiPrep, Metuchen, NJ) spectrofluorimeter. Excitation was at 280 nm. An inert argon atmosphere was maintained in the sample cell all over the measurements.

Stopped-flow kinetics

Kinetic measurements were performed at 20 ± 0.5°C on a DX 17MV stopped-flow (Applied Photophysics, Leatherhead, Surrey, United Kingdom) instrument using fluorescence detection as previously described (30). To preserve anaerobic conditions, the stopped-flow apparatus was in a glove-box with an atmosphere of purified nitrogen (quality 4.6). All reported concentrations of reactants correspond to those after mixing. In association experiments, pseudo-first-order conditions were ensured by applying Zn^{2+}concentrations at least 10-fold larger than the peptide concentration. Typically, 4–7 individual time courses were recorded under the same experimental conditions, for each evaluation. At pH 5.6 and 6.8, measurements were carried out in two different buffers to check the absence of buffer effects. Dilution experiments were performed to follow the dissociation reaction directly. A solution of Zn^{2+}-peptide complex in a 1 ml syringe was mixed with buffer in a 2.5 ml syringe, providing a 3.5 dilution factor. In these conditions, significant Zn^{2+} dissociation was observed only at pH ≤ 6.0.

pH indicator experiment

Kinetic experiments at pH 6.8 using Bromothymol Blue as a pH indicator ($pK_a = 7$) were performed with the above described stopped-flow instrument using absorption detection (model No. R928 photomultiplier, Hamamatsu, Hamamatsu City, Japan). The light source was a 250 W Tungsten lamp (Osram, Munich, Germany). Kinetics was monitored at 450 nm (absorption maximum of the acidic form of Bromothymol Blue), 494 nm (isosbestic point), and 615 nm (absorption maximum of the basic form of Bromothymol Blue).

Kinetic data analysis

The apparent rate constants k_{obs} and the amplitudes were determined from the kinetic data by extrapolating the kinetic phase to the true time zero by taking in account the experimentally determined dead time of 1.6 ms (34). All time-resolved kinetic phases could be analyzed with a monoexponential function. All fittings were carried out with the Origin (Microcal, Northampton, MA) software based on the nonlinear least-square method applying the Levenberg-Marquardt algorithm. All equilibrium constants are expressed as association constants.

RESULTS

Zn^{2+} binding kinetics at a single pH value

Since the Zn^{2+} binding information is fully encoded by the zinc fingers (8), the (35–50)NCp7 peptide (Fig. 1) corresponding to the distal finger of NCp7 has been selected as a relevant model (9). The dynamics of Zn^{2+} binding to (35–50) NCp7 is investigated under pseudo-first-order conditions by the fluorescence stopped-flow technique in anaerobic conditions, as previously described (30). In Fig. 2 *a*, the measured time course upon rapid mixing of 1.5 μM (35–50)NCp7 with 350 μM $Zn(ClO_4)_2$ in 50 mM MES pH 6.8 is shown as a representative example. The time-resolved kinetic phase can be fitted to a monoexponential function providing one observed rate constant k_{obs}. Experiments at different Zn^{2+} concentrations indicate a saturation behavior of k_{obs} (Fig. 2 *b*) and not the linear Zn^{2+} concentration-dependence associated to a one-step reaction that was previously observed for the point-mutated peptides (30). This saturation behavior is consistent with a two-step reaction scheme, where a rate-limiting interconversion step is coupled to a much faster, preceding binding step, considered as a preequilibrium:

$$L + Zn^{2+} \overset{K_M^*}{\rightleftharpoons} LZn^{2+*} \underset{k_b}{\overset{k_f}{\rightleftharpoons}} LZn^{2+}. \qquad (1)$$

Consequently, a comparatively stable intermediate complex, LZn^{2+*}, is postulated. By fitting the Zn^{2+}concentration dependence of k_{obs} to (35)

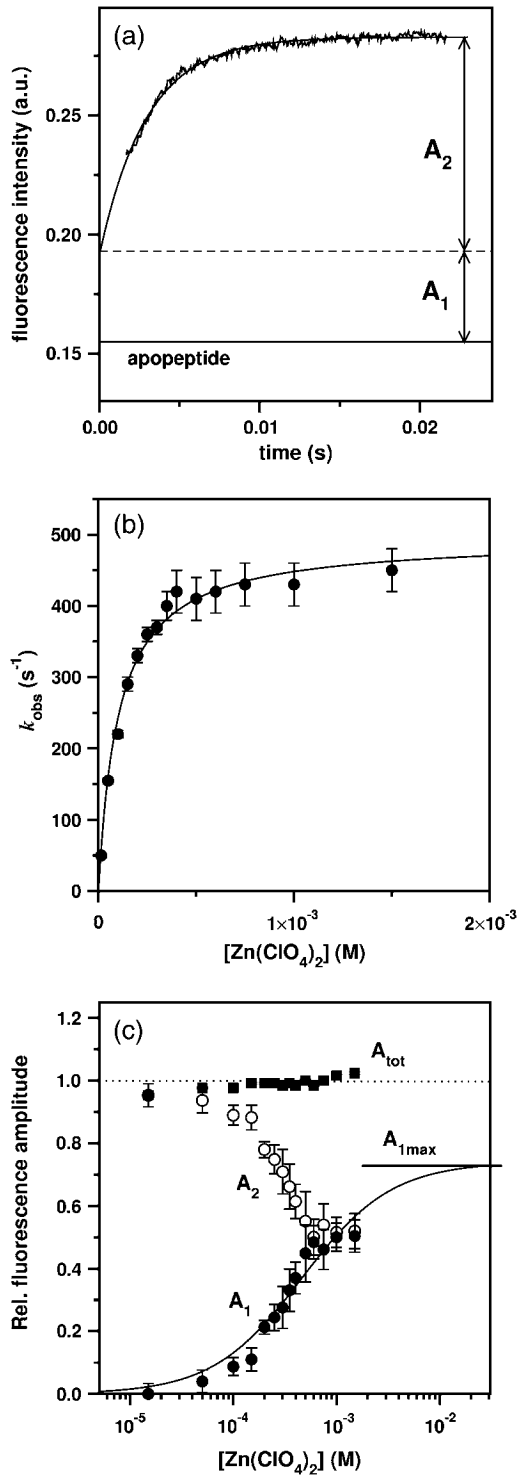

FIGURE 2 Zn^{2+} binding kinetics to (35–50)NCp7 at pH 6.8. The peptide was 1.5 μM in 50 mM HEPES/NaOH pH 6.8 at a total ionic strength of 0.15 M. (*a*) Representative kinetic experiment. Rapid mixing of the peptide with 0.35 mM $Zn(ClO_4)_2$ is performed at 20°C. The solid line is the best fit to a monoexponential function with $k_{obs} = 330\ s^{-1}$. A dead time of 1.6 ms is taken into account (see Materials and Methods). The concentrations are those after mixing. The fluorescence of the apopeptide is indicated. A_1 and A_2 are the amplitudes of the non-time-resolved and time-resolved processes, respectively. (*b*) Dependence of k_{obs} on the total Zn^{2+} concentration. The solid line is the best fit to the experimental data according to Eq. 2 with $k_f = 500\ s^{-1}$ and $K_M^* = 9000\ M^{-1}$. (*c*) Dependence of the relative fluorescence amplitudes on the total Zn^{2+} concentration: A_1, ●, A_2, ○, and total amplitude A_{tot}, ■. The dashed line indicates the fluorescence of the final complex. A_{1Max} is the non-time-resolved amplitude at high $[Zn(ClO_4)_2]$. The solid line is the best fit to the A_1 values using Eq. 3 with $K_M^* = (3 \pm 1) \times 10^3 M^{-1}$ and $A_{1Max} = 0.74 \pm 0.05$.

$$k_{obs} = \frac{k_f K_M^* [Zn^{2+}]}{1 + K_M^* [Zn^{2+}]} + k_b, \quad (2)$$

a value of $(9 \pm 1) \times 10^3\ M^{-1}$ is obtained for K_M^*, the association equilibrium constant of the LZn^{2+*} complex, and a value of $500 \pm 20\ s^{-1}$ is obtained for the sum of the forward (k_f) and backward (k_b) interconversion rate constants. The value of k_b, given by the intercept, is very low ($<0.1\ s^{-1}$) and cannot be determined from the experimental data. Thus, the value of $500\ s^{-1}$ corresponds essentially to k_f.

According to the two-step reaction scheme, a fast unresolvable process attributed to the formation of LZn^{2+*} is expected. In line with this expectation, the fluorescence intensity at the onset of the time-resolvable process is always markedly higher than the fluorescence intensity of the apopeptide (Fig. 2 *a*). The amplitudes of the nonresolvable and the resolvable processes are denoted A_1 and A_2, respectively (Fig. 2, *a* and *c*), and their sum represents the total amplitude change A_{tot}. In our conditions, A_{tot} is nearly independent of the Zn^{2+} concentration (Fig. 2 *c*), indicating that the final Zn^{2+}-ligand complex is formed completely even at the lowest Zn^{2+} concentration. On the other hand, A_1 clearly increases with the Zn^{2+} concentration and reaches a plateau value, A_{1Max}, corresponding to the fluorescence of the LZn^{2+*} complex. The Zn^{2+} concentration dependence of A_1 can be used to determine the equilibrium association constant, K_M^*, of LZn^{2+*}, according to

$$A_1 = \frac{K_M^* [Zn^{2+}] A_{1Max}}{1 + K_M^* [Zn^{2+}]}. \quad (3)$$

The obtained K_M^* value of $(3 \pm 1) \times 10^3\ M^{-1}$ is in agreement with the one obtained from the Zn^{2+} concentration dependence of k_{obs} (Fig. 2 *b*), demonstrating the consistency between kinetic and thermodynamic parameters.

pH dependence of the kinetic parameters

Since deprotonation reactions are involved in the Zn^{2+} binding reaction (9), the kinetic experiments were carried out between pH 5.2 and pH 8.5. The pH dependence of the forward interconversion rate-constant k_f is displayed in Fig. 3 *a*. Surprisingly, the highest k_f value ($\approx 850\ s^{-1}$) is observed at the lowest investigated pH; then k_f decreases with increasing pH. According to Eq. 2, the K_M^* values, determined from the Zn^{2+} concentration dependences of k_{obs}, are also pH-dependent (Fig. 3 *b*). The resulting slope is 1.35 ± 0.02 indicating that Zn^{2+}-binding requires the deprotonation of one to

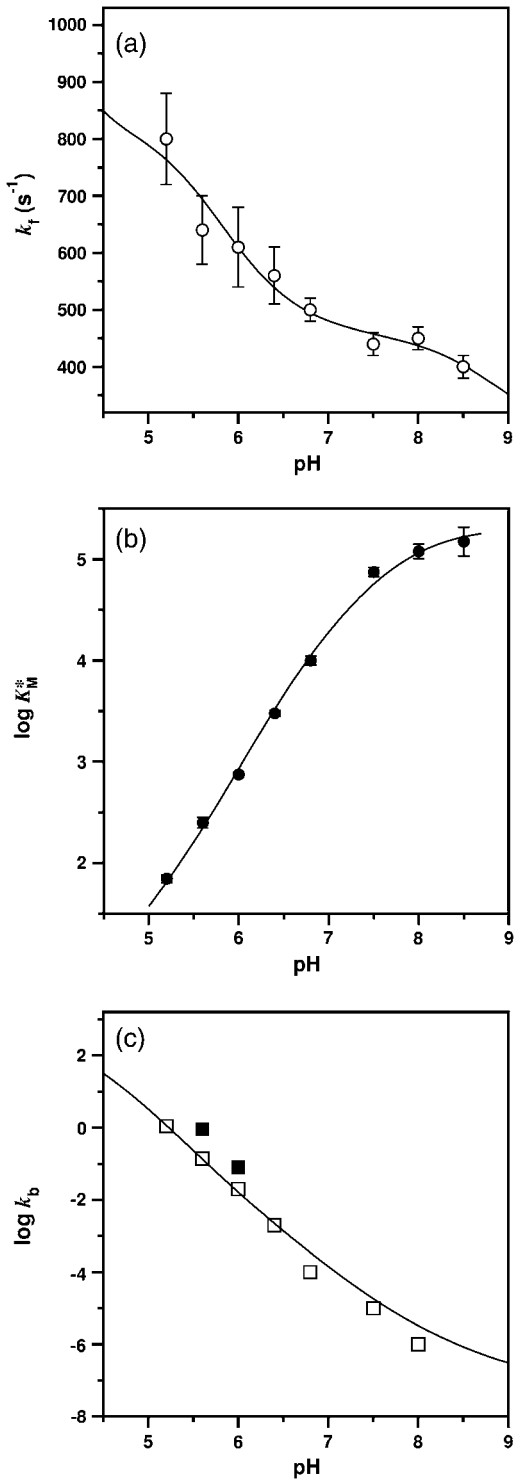

FIGURE 3 pH-dependence of Zn^{2+} binding to (35–50)NCp7. (*a*) Forward interconversion step k_f, ○. The solid line is the best fit to the experimental points using Eq. 8 with the k_{fi} parameters in Table 1. (*b*) Equilibrium constant K^*_M. The solid line is the best fit according to Eq. 6 and the K_{H1}, K_{H2}, K^*_{M1}, and K^*_{M2} values in Table 1. (*c*) Backward interconversion step k_b, ■; and experimental values, □, calculated values according to Eq. 5. The solid line is the best fit using Eq. 9 and the K_{MH2}, K_{MH3}, K_{MH4}, k_{b1}, k_{b2}, k_{b3}, and k_{b4} values of Table 1.

two Zn^{2+} coordinating residues before the rate-limiting step. Since the peptide contains four Zn^{2+} coordinating residues, additional deprotonation steps are expected to occur subsequently to the rate-limiting step.

Due to its low value, the backward interconversion rate constant k_b can be determined by dilution-induced dissociation experiments (34) only at low pH from

$$k_{obs} = \frac{k_f}{1 + \dfrac{3.5}{K^*_M[Zn^{2+}]_{Tot}}} + k_b, \quad (4)$$

where $[Zn^{2+}]_{Tot}$ is the total, i.e., free and bound, concentration of Zn^{2+} in the syringe containing the Zn^{2+} bound peptide. We obtained 0.9 s^{-1} and 0.08 s^{-1} for k_b at pH 5.6 and 6.0, respectively, indicating that the dissociation rate is also pH-dependent (Fig. 3 *c*). Alternatively, under the condition $k_f/k_b \gg 1$, the k_b value can be calculated from the overall Zn^{2+} binding equilibrium constant K_{app} (9) according to

$$k_b = \frac{K^*_M k_f}{K_{app}}. \quad (5)$$

The acceptable agreement between the calculated and measured values of k_b at pH 5.6 and 6.0 (Fig. 3 *c*) gives confidence to the calculated values of k_b and their pH dependence.

The linear part of the curve in Fig. 3 *c* is characterized by a slope of 2.2 ± 0.1, indicating that protonation of two Zn^{2+} coordinating groups takes place before the rate-limiting dissociation step k_b. Based on the principle of microscopic reversibility, two corresponding fast deprotonation steps have to occur also in the opposite direction, namely subsequent to the rate-limiting binding step, k_f. Because these steps are much faster than the rate-limiting binding step, they cannot affect the k_f value. Conversely, it should be possible to detect this rate-limiting step through the pH change originating from the subsequent deprotonation. To this purpose, a stopped-flow experiment with absorption detection was performed by mixing (35–50)NCp7 with $Zn(ClO_4)_2$ in 5 mM MES pH 6.8 in the presence of Bromothymol Blue as a suitable pH indicator. In line with our hypothesis, a time-resolvable process was observed (Fig. 4) with a k_{obs} of 235 s^{-1}, very close to that found for Zn^{2+} binding. This result indicates that cation binding and the pH change revealed by the indicator are controlled by the same rate-limiting step. Due to the very fast protonation and deprotonation reactions, this feature confirms that the protons are released by the deprotonation reactions subsequent to the rate-limiting Zn^{2+} binding step. In further agreement with the above conclusions, the amplitude of the absorption change of the indicator shows that one to two protons are released per bound Zn^{2+}, subsequent to the rate-limiting step at pH 6.8.

Since the binding of Zn^{2+} to (35–50)NCp7 leads to fluorescent intermediates, the pH dependence of their fluorescence intensity is compared with the pH dependence of the fluorescence intensities of the Zn^{2+}-bound peptide and apopeptide (Fig. 5). At low pH, the fluorescence level of the

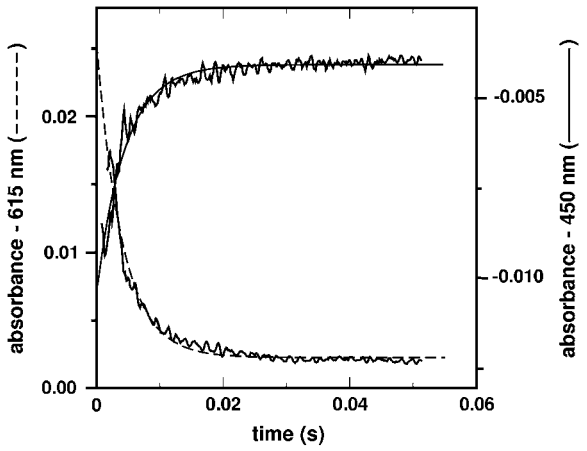

FIGURE 4 Proton release coupled to the rate-limiting reaction step. 150 μM (35–50)NCp7 was mixed with 100 μM $Zn(ClO_4)_2$ in 5 mM MES/NaOH pH 6.8 at 20°C and a total ionic strength of 0.15 M. Time-resolved absorption of the pH indicator Bromothymol Blue (15 μM), observed at (*a*) 450 nm (acidic state) and (*b*) 615 nm (basic state). The theoretical curves (*solid* and *dashed lines*) correspond to a monoexponential function with $k_{obs} = 235\ s^{-1}$. The concentrations refer to conditions after mixing.

intermediates is close to that of the apopeptide, whereas at high pH, it approaches that of the final complex. The marked fluorescence change in the pH range from 5 to 8 indicates that the intermediates display various protonation states differing by their quantum yields.

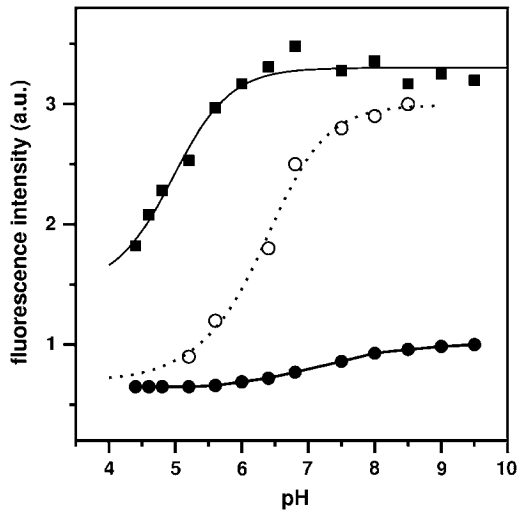

FIGURE 5 pH-dependence of the fluorescence intensities of the different (35–50)NCp7 forms. Apopeptide, ●; intermediate Zn^{2+}-complex, ○; and final Zn^{2+}-complex, ■. The fluorescence intensities of the intermediates are obtained from the non-time-resolved amplitudes in the kinetic traces (Fig. 2). The dotted line is the best fit using Eq. 7 and the K^*_{MH2} and K^*_{MH3} values of Table 1. The fluorescence of the final Zn^{2+}-complex, corresponding to A_{tot} in the kinetic traces, and its fit (*solid line*) are from our previous work (9).

DISCUSSION

Thermodynamic and kinetic parameters of Zn^{2+} binding to (35–50)NCp7

In our previous article (30), we investigated the kinetics of Zn^{2+} binding and dissociation to two point-mutated peptides of the distal CCHC motif of NCp7. The complex formation was analyzed on the basis of a multistep reaction model involving three Zn^{2+} binding paths due to three deprotonated states of the coordinating motif, acting as monodentate, bidentate, and tridentate ligands. The rate constants for the intermolecular binding paths of the bidentate and tridentate states were much smaller than expected according to electrostatic considerations (36). This was attributed to conformational constraints required to achieve the proper metal coordination during folding. In addition, intermediates were found to be involved in the reaction path. Based on the reaction scheme that was developed for Zn^{2+} binding to the tridentate-mutated peptides (30), one could simply expect that, in the intact tetradentate (35–50)NCp7 peptide, the reaction model has to be expanded by introducing one additional binding step, due to the additional coordinating residue. Since the associated Zn^{2+} binding rate constant for the fully deprotonated (35–50)NCp7 peptide would have been as high as $7 \times 10^9\ M^{-1}\ s^{-1}$ according to the model of Fuoss (36), the corresponding reaction step would not be resolvable by the stopped-flow method under our experimental conditions. On the contrary, we find a resolvable kinetic reaction phase in the millisecond time range. Therefore, as it was previously observed with the tridentate mutated peptides, the binding rate constant of the native (35–50)NCp7 peptide at high pH is lower than theoretically predicted. In addition, both the significant amplitude of the fast, non-time-resolvable process in the kinetic traces of the native peptide (Fig. 2 *a*) and the saturation behavior of the Zn^{2+} concentration dependence of k_{obs} (Fig. 2 *b*) at all investigated pH values indicate that a comparatively stable intermediate is formed before the rate-limiting interconversion step. A possible assignment of the slow interconversion to a protonation reaction is excluded since the rate constant of the transition is independent of the buffer concentration, as it was shown at pH 6. Therefore, this process is attributed to a conformational change of the ligand subsequent to the initial binding process.

To determine the kinetic parameters in terms of single reaction steps, the reaction scheme in Fig. 6 is considered. Due to the four coordinating residues, there are five protonation states of the apopeptide. The fully protonated LH_4^+ species is assumed not to coordinate Zn^{2+} because of unfavorable electrostatics. Due to the pH dependence of the fluorescence of the intermediates (Fig. 5), we postulate different protonation states: $LH_3{*}Zn^{2+}$ to $L{*}Zn^-$ with coordination numbers (in respect to the binding of the peptide coordinating residues) that cannot be predicted a priori. However, we can assume that $LH_3{*}Zn^{2+}$ exhibits a coordination number of one. Finally, four states of the final Zn^{2+} complex,

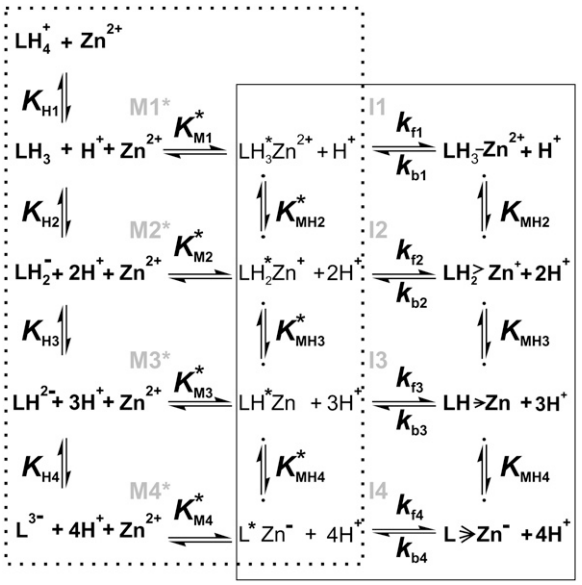

FIGURE 6 Reaction scheme for Zn^{2+} binding to (35–50)NCp7. K_{Hi}, K^*_{MHi}, and K_{MHi} correspond to the equilibrium protonation constants of the apopeptide, the intermediate, and the final complexes, respectively. K^*_{MHi} are the stability constants for the intermediate complexes while k_{fi} and k_{bi} are the forward and backward rate constants, respectively, of the i^{th} interconversion step. The equilibrium constants of the interconversion steps are defined as $K_{Ii} = k_{fi}/k_{bi}$. The overall Zn^{2+} binding constants for each final complex, K_{Mi}, are from our previous work (9) and correspond to $K_{Mi} = K^*_{Mi} \times K_{Ii}$. The reactions within the dotted contour are used to derive Eq. 6, while the reactions within the continuous contour are used to derive Eqs. 8 and 9.

differing in coordination number, are considered: LH_3Zn^{2+} to LZn^-.

As for the mutated peptides (30), several reaction schemes of increased complexity have been considered to fit our data. All reaction schemes including only a reduced number of final or intermediate complexes (i.e., less than four $LH_nZn^{(n-1)}$ or $LH_n{*}Zn^{(n-1)}$ states) failed to properly fit the data on the kinetics of Zn^{2+} binding and dissociation of the native (35–50)NCp7 peptide, and were thus excluded. Therefore, the data have been analyzed on the basis of the whole reaction scheme, using the previously determined protonation constants of the apopeptide (K_{Hi}) and holopeptide (K_{MHi}) as well as the binding constants (K_{Mi}) associated with the overall formation of each final Zn^{2+} complex (9).

Since our data indicate that the reactions leading to the intermediate complexes (*left side* of Fig. 6) are much faster than the subsequent rate limiting reactions leading to the final complexes (*right side* of Fig. 6), we assume that the reactions on the left have reached an equilibrium before the interconversion reactions on the right take place. As a consequence, the pH dependence of the stability constant of the intermediates, K^*_M, can be described by using only the reactions within the dotted contour while the interconversion rate constants k_f and k_b can be analyzed through the reaction scheme within the solid contour.

Thermodynamic parameters from the pH dependence of the stability constant and the fluorescence intensity of the intermediates

Since the deprotonation of two groups appears to account for the pH dependence of K^*_M, the data in Fig. 3 *b* are fitted by Eq. 6 based on a model including only two metal binding steps:

$$K^*_M = \frac{K^*_{M2} + K^*_{M1}K^*_{MH2}[H^+]}{1 + K_{H2}[H^+] + K_{H2}K_{H1}[H^+]^2}. \quad (6)$$

Due to the steep pH dependence of K^*_M below pH 8, only the two more acidic protonation constants, K_{H1} and K_{H2} of the apopeptide, likely contribute to this pH dependence. Therefore, the binding steps involved in the pH dependence of K^*_M are attributed to M1* and M2* (Fig. 6). Values of $(1.3 \pm 0.6) \times 10^3\ M^{-1}$ and $(2.0 \pm 0.5) \times 10^5\ M^{-1}$ are found for K^*_{M1} and K^*_{M2}, respectively (Table 1). K^*_{M1} is very similar to K_{M1} associated with the overall binding step M1 determined in Bombarda et al. (9), indicating that the interconversion equilibrium constant $K_{I1} = k_{f1}/k_{b1} = K_{M1}/K^*_{M1}$ is $\sim$1 and thus, the step I1 does not stabilize the final complex LH_3Zn^{2+}. This result is consistent with the hypothesis that only one coordination is involved both in $LH_3{*}Zn^{2+}$ and LH_3Zn^{2+}, a constraint that is probably not sufficient to reorganize and stabilize the peptide. In contrast, K^*_{M2} is approximately two orders-of-magnitude smaller than K_{M2} associated to the overall binding step M2, implying that $K_{I2} = k_{f2}/k_{b2} = K_{M2}/K^*_{M2} = 150$ and thus, the step I2 substantially stabilizes the final LH_2Zn^+ complex. Moreover, from Fig. 6 the equilibrium constant, K^*_{MH2} relating the $LH_2{*}Zn^+$ and $LH_3{*}Zn^{2+}$species, can be calculated by $K^*_{MH2} = K_{H2} \times K^*_{M1}/K^*_{M2}$. A value of $5 \times 10^5\ M^{-1}$ is obtained, indicating that as for the final complexes (9), the repulsive electrostatic interactions between the bound cation and the protons decrease the protonation constant in respect to that of the free peptide ($K_{H2} = 10^8\ M^{-1}$).

Additional equilibrium constants can be extracted from the pH dependence of the fluorescence intensity of the intermediates (Fig. 5). This pH dependence is attributed to various protonation states of the intermediates (Fig. 6) differing by their quantum yields. Since the quantum yields are strongly related to peptide folding (31), the least protonated intermediates LH*Zn and $L{*}Zn^-$ with probably the highest coordination number are assumed to be the most folded and thus, the most fluorescent intermediates. In contrast, the $LH_3{*}Zn^{2+}$ complex with coordination number 1 is likely almost unfolded and thus exhibits the same fluorescence as the apopeptide. Two protonation steps are needed to describe the pH dependence of the fluorescence intensity of the intermediates. These steps are interpreted as the ones characterized by the equilibrium constants, K^*_{MH2} and K^*_{MH3}. The following equation is used,

$$I = \frac{I_{LH_3{*}Zn} + I_{LH_2{*}Zn}K^*_{MH2}[H^+] + I_{LH{*}Zn}K^*_{MH2}K^*_{MH3}[H^+]^2}{1 + K^*_{MH2}[H^+] + K^*_{MH2}K^*_{MH3}[H^+]^2}, \quad (7)$$

TABLE 1 Equilibrium and kinetic parameters of Zn^{2+} binding to (35–50)NCp7 at 20°C

Step i	K_{Hi} (M^{-1})†	K_{Mi} (M^{-1})†	K^*_{Mi}(M^{-1})	K^*_{Mi}(M^{-1})	k_{fi} (s^{-1})	k_{bi} (s^{-1})	K_{Ii}	K_{MHi} (M^{-1})†
1	3×10^6	1×10^3	$(1.3 \pm 0.6) \times 10^3$	—	850 ± 50	1000	0.8	—
2	1×10^8	3×10^7	$(2.0 \pm 0.5) \times 10^5$	$(6 \pm 3) \times 10^5$	500 ± 50	3 ± 1	1.5×10^2	3×10^3
3	6×10^8	9×10^{11}	1.2×10^7	$(1.0 \pm 0.5) \times 10^7$	450 ± 50	$(9 \pm 3) \times 10^{-3}$	7×10^4	2×10^4
4	3×10^9	2.7×10^{16}	4.5×10^7	$(8.0 \pm 0.3) \times 10^8$	300 ± 200	10^{-7}	6×10^8	1.0×10^5

The parameters are defined in Fig. 6 and determined as described in the text.
†Values from our previous work (9).

where I_{LH^*Zn}, $I_{LH_2{}^*Zn}$, and $I_{LH_3{}^*Zn}$ are the fluorescence intensities of LH*Zn, $LH_2{}^*Zn^+$, and $LH_3{}^*Zn^{2+}$, respectively. Values of $(6 \pm 3) \times 10^5$ M^{-1} and $(1.0 \pm 0.5) \times 10^7$ M^{-1} are obtained for K^*_{MH2} and K^*_{MH3}, respectively. The K^*_{MH2} value is in good agreement with the value inferred from the pH dependence of K^*_M, corroborating our attribution of the protonation steps. The I_{LH^*Zn} value is assumed to correspond to the fluorescence plateau at high pH (Fig. 5). Since this intensity is only 10% lower than that of the final holopeptide, the fluorescence and thus, the folding of L^*Zn^- and LH*Zn are expected to be similar, explaining why the transition between these two intermediates cannot be monitored in Fig. 5.

With the knowledge of K^*_{M3}, we determine $K^*_{M3} = K^*_{M2} \times K_{H3}/K^*_{MH3} = 1.2 \times 10^7$ M^{-1} on the basis of Fig. 6. K^*_{M3} is two and four orders of magnitude higher than K^*_{M2} and K^*_{M1}, respectively, suggesting that the coordination number incrementally increases in the corresponding intermediates. Since Zn^{2+} is assumed to be singly coordinated in $LH_3{}^*Zn^{2+}$, the coordination numbers of $LH_2{}^*Zn^+$ and LH*Zn are likely 2 and 3, respectively. Moreover, from K^*_{M3} and the previously (9) determined K_{M3} (9×10^{11} M^{-1}), it can be further concluded that $K_{I3} = K_{M3}/K^*_{M3} = 7 \times 10^4$, indicating that the step I3 significantly stabilizes the complex.

Thermodynamic and kinetic parameters from the pH dependence of the interconversion rate constants

As explained above, the equations to describe the pH dependence of the forward and backward interconversion constants, k_f and k_b, respectively, can be derived from the right part of Fig. 6:

$$k_f = \frac{k_{f1}K^*_{MH2}K^*_{MH3}K^*_{MH4}\times 10^{-3pH} + k_{f2}K^*_{MH3}K^*_{MH4}\times 10^{-2pH} + k_{f3}K^*_{MH4}\times 10^{-pH} + k_{f4}}{1 + K^*_{MH4}\times 10^{-pH} + K^*_{MH3}K^*_{MH4}\times 10^{-2pH} + K^*_{MH2}K^*_{MH3}K^*_{MH4}\times 10^{-3pH}}, \quad (8)$$

$$k_b = \frac{k_{b1}K_{MH2}K_{MH3}K_{MH4}\times 10^{-3pH} + k_{b2}K_{MH3}K_{MH4}\times 10^{-2pH} + k_{b3}K_{MH4}\times 10^{-pH} + k_{b4}}{1 + K_{MH4}\times 10^{-pH} + K_{MH3}K_{MH4}\times 10^{-2pH} + K_{MH2}K_{MH3}K_{MH4}\times 10^{-3pH}}. \quad (9)$$

By fixing K^*_{MH2} and K^*_{MH3} to the values determined above, the fit of the k_f data (Fig. 3 *a*) with Eq. 8 provides $k_{f1} = 850 \pm 50$ s^{-1}, $k_{f2} = 500 \pm 50$ s^{-1}, $k_{f3} = 450 \pm 50$ s^{-1}, and $K^*_{MH4} = (8.0 \pm 0.3) \times 10^8$ M^{-1}. Due to its large value, K^*_{MH4} is probably associated with the deprotonation of Cys^{49}, which is thought to be the last coordinating residue in the stepwise coordination of Zn^{2+} (9). By fixing $K^*_{MH4} = 8.0 \times 10^8$ M^{-1} in Eq. 8, it is possible to extrapolate $k_{f4} = 300 \pm 200$ s^{-1}, which represents the value of k_f at high pH. The equilibrium constant K^*_{MH4} is lower than K_{H4} (3×10^9 M^{-1}) in the apopeptide as expected from the additional acidity provided by the coordinated Zn^{2+}; however, the difference is small. A consequence of the similarity of the K^*_{MH4} and K_{H4} values is that $K^*_{M4} = K^*_{M3} \times K_{H4}/K^*_{MH4} = 4.5 \times 10^7$ M^{-1}. The close values of K^*_{M4} and K^*_{M3} indicate that Zn^{2+} is bound with similar affinity and thus, probably with the same coordination number 3 in LH*Zn and L^*Zn^-, in line with their similar associated fluorescence. These considerations support the hypothesis that at high pH, even if deprotonated, Cys^{49} does not bind Zn^{2+} in L^*Zn^- and thus a water molecule remains in the coordination sphere of Zn^{2+} in this complex. Moreover, from K^*_{M4} and the previously determined K_{M4} value (2.7×10^{16} M^{-1}), it can be further concluded that $K_{I4} = K_{M4}/K^*_{M4} = 6 \times 10^8$, indicating that the step I4 considerably stabilizes the final complex. Since Zn^{2+} is coordinated exclusively by all four residues in the last complex (6,37), this interconversion step, besides accounting for the structural rearrangement necessary to bring Cys^{49} into the required position for subsequent binding (as in the step I3), implies also the binding of the deprotonated Cys^{49} and the substitution of the remaining Zn^{2+} bound water. Finally, from the K_{Ii} and k_{fi} values, the backward rate constants k_{bi} can be calculated by $k_{bi} = k_{fi}/K_{Ii}$. Values of 1000 s^{-1}, 3 s^{-1}, 6×10^{-3} s^{-1}, and 5×10^{-7} s^{-1} are obtained for k_{b1}, k_{b2}, k_{b3} and k_{b4}, respectively.

In a next step, the pH dependence of k_b in Fig. 3 *c* was fitted to Eq. 9, by fixing the protonation constants of the final Zn^{2+}-bound complexes, K_{MH2} to K_{MH4}, to the values determined previously (9). Due to the low K_{MH2} value, k_{b1} does not contribute to k_b in the investigated pH range and cannot be determined. Moreover, the fits and various simulations show that only an upper limit can be obtained for k_{b4}

($\leq 10^{-7}$ s^{-1}). In contrast, both k_{b2} (3 ± 1 s^{-1}) and k_{b3} ($9 \pm 3 \times 10^{-3}$ s^{-1}) are recovered more confidently and are in agreement with the values inferred from K_{Ii} and k_{fi}. Furthermore, the comparison of the upper limit of k_{b4} with the value calculated from K_{I4} and k_{f4} suggests that a reasonable estimate of k_{b4} is 10^{-7} s^{-1}.

All the kinetic and equilibrium constants are reported in Table 1. Since all the parameters in Fig. 6 are linked together, we have checked whether the reported values are consistent with the complete reaction scheme in Fig. 6. For instance, we have notably checked whether a given equilibrium constant assumes the same value when it is calculated using alternative expressions involving different parameters. Despite the complexity of the model, no deviation larger than a factor of 6 is observed on each individual value, demonstrating the full consistency between the thermodynamic and kinetic parameters. Due to the large number of parameters and the overdetermination of the system, this stringent criterion gives a high confidence to our model.

Proposed molecular mechanism of Zn^{2+} induced folding of (35–50)NCp7

Coordination of a solvated metal ion by a ligand proceeds generally via the fast formation of an outer-sphere complex between the solvated cation and the ligand; then the substitution of the first water molecule by one coordinating atom of the ligand leads to inner-sphere coordination. The substitution of the first solvate water molecule is rate-limiting only if the binding of further ligand atoms is significantly faster. This feature requires substantial ligand flexibility because the rearrangement of the ligand conformation, necessary to bring the next coordinating atoms into the required position, must be faster than the subsequent substitution of the remaining solvate water molecules. This is obviously not the case for the binding of Zn^{2+} to (35–50)NCp7, since one of the most striking aspects of our data is the evidence of intermediate complexes and their slow conversion to the final complexes. With the exception of L^*Zn^-, the intermediates do not seem to change their coordination number during the interconversion step, which thus corresponds to a conformational rearrangement. The precise nature of this rearrangement is difficult to assess. Nevertheless, since both LH^*Zn and L^*Zn^- intermediates are inferred to be largely folded, their rearrangement consists likely of minor structural changes that provide strong stabilization, as shown by both K_{I3} and K_{I4} (Table 1). Due to the highly constrained structure adopted by the peptide when all four coordinating residues are bound to Zn^{2+} (6,7,37), the coordination degree of 3 inferred for L^*Zn^- suggests that the peptide flexibility is not sufficient to bring rapidly the fourth coordinating residue (Cys^{49}) into the required position to bind the metal. The structure of L^*Zn^- as well as that of the other intermediates is likely not optimized and needs to be rearranged to yield a form more suitably folded to rapidly lead to the native form. In this respect, the interconversion step may be viewed as a rearrangement of the peptide backbone around Zn^{2+} to optimize the binding geometry. Consequently, the decrease of k_f with the coordination degree of the intermediates is probably due to increasing constraints within the peptide that slow down the structural rearrangement.

In the previously studied point-mutated peptides, due to the absence of one coordinating residue, the constraints within the peptide are reduced and the optimized constrained native folded state cannot be reached (30,38). Consequently, the rearrangement step can proceed more rapidly than in the tetradentate native peptide. Additionally, the lack of one coordinating group likely lowers the stability of the intermediates in the tridentate-mutated peptides. Due to this lower stability, the saturation behavior of k_{obs} in the point-mutated

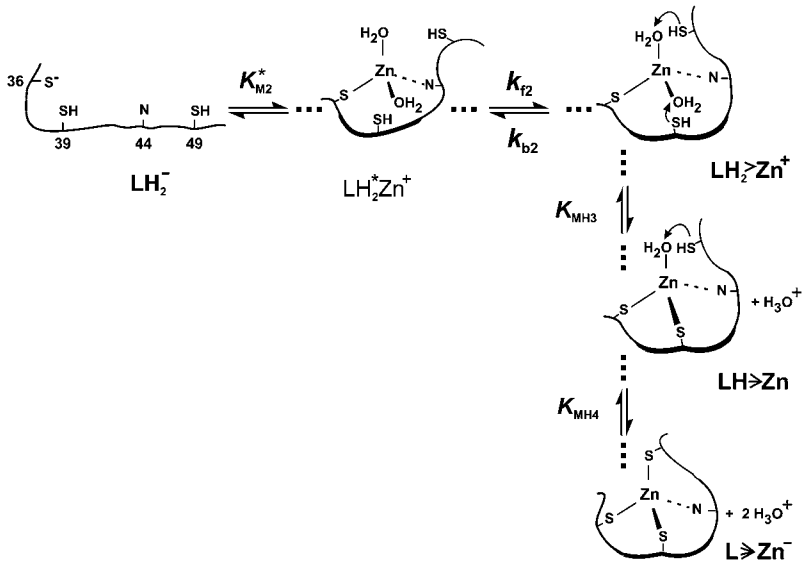

FIGURE 7 Proposed mechanism of Zn^{2+} coordination and induced folding of (35–50)NCp7 in the neutral pH range. Only the species that are most relevant for Zn^{2+} binding and dissociation are shown. The rate-limiting interconversion step between $LH_2{*}Zn^+$ and LH_2Zn is assumed to correspond to a rearrangement of the peptide backbone enabling the formation of an adequately folded form that rapidly leads to the final LZn^- complex.

peptides would be observable only at comparatively high Zn^{2+} concentrations, where the k_{obs} values are too fast to be determined. These features imply that the intermediates cannot accumulate in the point-mutated peptides, explaining why they have not been observed.

From our data, a molecular model (Fig. 7) could be proposed to describe the major pathway for the Zn^{2+}-driven folding of (35–50)NCp7. The final Zn^{2+} complex cannot markedly form via LH^{2-}, L^{3-}, and L^*Zn^- since these species are not much populated at neutral pH, due to the high K_{H3}, K_{H4}, and K^*_{MH4} values. Moreover, due to the low K^*_{M1} ($1.3 \times 10^3 M^{-1}$) and K_{I1} (0.8) values associated with the binding of Zn^{2+} to LH_3 where only His^{44} is thought to be deprotonated, this species cannot play an important role at Zn^{2+} concentrations in the micromolar range or lower. Thus, the complex formation will mainly start with the bidentate LH_2^- species where both His^{44} and Cys^{36} residues are deprotonated. Binding of both residues to Zn^{2+} gives the $LH_2{*}Zn^+$ intermediate. Since the slopes of the pH dependence of K^*_M, k_f, and k_b (Fig. 3) show that two deprotonation reactions occur prior and subsequent to the rate-limiting conformational changes, the $LH_2{*}Zn^+$ intermediate is likely converted into the appropriately folded LH_2Zn^+ species. Then, the final LZn^- complex is rapidly generated through deprotonation of Cys^{39} and Cys^{49} residues. This rapid conversion into LZn^- necessarily implies that the Cys^{39} and Cys^{49} residues are close to Zn^{2+} in LH_2Zn^+, so that they can readily substitute the remaining solvate molecules. In the other direction, the release of Zn^{2+} from the final complex LZn^- does not occur efficiently via L^*Zn^- or LH*Zn, since k_{b4} and k_{b3} are by orders of magnitude lower than k_{b2}. Therefore, we propose that dissociation starts by protonation of the final complex to provide LH_2Zn^+, and then proceeds via $LH_2{*}Zn^+$ to the apopeptide.

This study constitutes the first quantitative molecular model of the Zn^{2+}-triggered folding mechanism of a CCHC zinc finger. With the exception of initial studies on CCHH zinc fingers (39), no detailed report on the kinetics of metal binding to a zinc finger peptide has been published so far. In the future, efforts should be made to further characterize the intermediates, which are critical to generate the folded zinc fingers. Since the activity of HIV-1 NCp7 strongly relies on its folded fingers, the intermediates are potential targets to inhibit NCp7.

We thank P. Buet and E. Lewitzki for helpful discussions and P. Petitjean for peptide synthesis.

E.B. is grateful to Deutscher Akademischer Austausch Dienst and Boehringer-Ingelheim Foundation for funding. Y.M. was supported by a von Humboldt fellowship. This work was supported by the Max-Plank-Society, Agence Nationale pour la Recherche contre le Sida, Sidaction and European Community (Targeting Replication and Integration of HIV integrated project).

REFERENCES

1. Berg, J. M., and Y. Shi. 1996. The galvanization of biology: a growing appreciation for the roles of zinc. *Science.* 271:1081–1085.
2. Cox, E. H., and G. L. McLendon. 2000. Zinc-dependent protein folding. *Curr. Opin. Chem. Biol.* 4:162–165.
3. Berg, J. M. 1986. Potential metal-binding domains in nucleic acid binding proteins. *Science.* 232:485–487.
4. Darlix, J. L., M. Lapadat-Tapolsky, H. de Rocquigny, and B. P. Roques. 1995. First glimpses at structure-function relationships of the nucleocapsid protein of retroviruses. *J. Mol. Biol.* 254:523–537.
5. Bess, J. W., Jr., P. J. Powell, H. J. Issaq, L. J. Schumack, M. K. Grimes, L. E. Henderson, and L. O. Arthur. 1992. Tightly bound zinc in human immunodeficiency virus type 1, human T-cell leukemia virus type I, and other retroviruses. *J. Virol.* 66:840–847.
6. Summers, M. F., L. E. Henderson, M. R. Chance, J. W. Bess, Jr., T. L. South, P. R. Blake, I. Sagi, G. Perez-Alvarado, R. C. Sowder, D. R. Hare, and L. O. Arthur. 1992. Nucleocapsid zinc fingers detected in retroviruses: EXAFS studies of intact viruses and the solution-state structure of the nucleocapsid protein from HIV-1. *Protein Sci.* 1:563–574.
7. Morellet, N., N. Jullian, H. De Rocquigny, B. Maigret, J. L. Darlix, and B. P. Roques. 1992. Determination of the structure of the nucleocapsid protein NCp7 from the human immunodeficiency virus type 1 by ^1H NMR. *EMBO J.* 11:3059–3065.
8. Mély, Y., H. De Rocquigny, N. Morellet, B. P. Roques, and D. Gérard. 1996. Zinc binding to the HIV-1 nucleocapsid protein: a thermodynamic investigation by fluorescence spectroscopy. *Biochemistry.* 35: 5175–5182.
9. Bombarda, E., N. Morellet, H. Cherradi, B. Spiess, S. Bouaziz, E. Grell, B. P. Roques, and Y. Mely. 2001. Determination of the pK_a of the four Zn^{2+}-coordinating residues of the distal finger motif of the HIV-1 nucleocapsid protein: consequences on the binding of Zn^{2+}. *J. Mol. Biol.* 310:659–672.
10. Darlix, J. L., C. Gabus, M. T. Nugeyre, F. Clavel, and F. Barre-Sinoussi. 1990. *Cis* elements and *trans*-acting factors involved in the RNA dimerization of the human immunodeficiency virus HIV-1. *J. Mol. Biol.* 216:689–699.
11. Tanchou, V., D. Decimo, C. Pechoux, D. Lener, V. Rogemond, L. Berthoux, M. Ottmann, and J. L. Darlix. 1998. Role of the N-terminal zinc finger of human immunodeficiency virus type 1 nucleocapsid protein in virus structure and replication. *J. Virol.* 72:4442–4447.
12. de Rocquigny, H., P. Petitjean, V. Tanchou, D. Decimo, L. Drouot, T. Delaunay, J. L. Darlix, and B. P. Roques. 1997. The zinc fingers of HIV nucleocapsid protein NCp7 direct interactions with the viral regulatory protein Vpr. *J. Biol. Chem.* 272:30753–30759.
13. Druillennec, S., A. Caneparo, H. de Rocquigny, and B. P. Roques. 1999. Evidence of interactions between the nucleocapsid protein NCp7 and the reverse transcriptase of HIV-1. *J. Biol. Chem.* 274:11283–11288.
14. Cristofari, G., and J. L. Darlix. 2002. The ubiquitous nature of RNA chaperone proteins. *Prog. Nucleic Acid Res. Mol. Biol.* 72:223–268.
15. Levin, J. G., J. Guo, I. Rouzina, and K. Musier-Forsyth. 2005. Nucleic acid chaperone activity of HIV-1 nucleocapsid protein: critical role in reverse transcription and molecular mechanism. *Prog. Nucleic Acid Res. Mol. Biol.* 80:217–286.
16. Chertova, E. N., B. P. Kane, C. McGrath, D. G. Johnson, R. C. Sowder 2nd, L. O. Arthur, and L. E. Henderson. 1998. Probing the topography of HIV-1 nucleocapsid protein with the alkylating agent *n*-ethylmaleimide. *Biochemistry.* 37:17890–17897.
17. Scozzafava, A., A. Mastrolorenzo, and C. T. Supuran. 2001. Agents that target cysteine residues of biomolecules and their therapeutic potential. *Exp. Opin. Ther. Pat.* 11:765–787.
18. Dorfman, T., J. Luban, S. P. Goff, W. A. Haseltine, and H. G. Gottlinger. 1993. Mapping of functionally important residues of a cysteine-histidine box in the human immunodeficiency virus type 1 nucleocapsid protein. *J. Virol.* 67:6159–6169.
19. Déméné, H., C. Z. Dong, M. Ottmann, M. C. Rouyez, N. Jullian, N. Morellet, Y. Mély, J. L. Darlix, M. C. Fournié-Zaluski, S. Saragosti, and B. P. Roques. 1994. 1H NMR structure and biological studies of the $His^{23} \rightarrow Cys$ mutant nucleocapsid protein of HIV-1 indicate that the

conformation of the first zinc finger is critical for virus infectivity. *Biochemistry.* 33:11707–11716.

20. Gorelick, R. J., S. M. Nigida, Jr., J. W. Bess, Jr., L. O. Arthur, L. E. Henderson, and A. Rein. 1990. Noninfectious human immunodeficiency virus type 1 mutants deficient in genomic RNA. *J. Virol.* 64:3207–3211.
21. Gorelick, R. J., T. D. Gagliardi, W. J. Bosche, T. A. Wiltrout, L. V. Coren, D. J. Chabot, J. D. Lifson, L. E. Henderson, and L. O. Arthur. 1999. Strict conservation of the retroviral nucleocapsid protein zinc finger is strongly influenced by its role in viral infection processes: characterization of HIV-1 particles containing mutant nucleocapsid zinc-coordinating sequences. *Virology.* 256:92–104.
22. Remy, E., H. de Rocquigny, P. Petitjean, D. Muriaux, V. Theilleux, J. Paoletti, and B. P. Roques. 1998. The annealing of tRNA3Lys to human immunodeficiency virus type 1 primer binding site is critically dependent on the NCp7 zinc fingers structure. *J. Biol. Chem.* 273: 4819–4822.
23. Guo, J., T. Wu, J. Anderson, B. F. Kane, D. G. Johnson, R. J. Gorelick, L. E. Henderson, and J. G. Levin. 2000. Zinc finger structures in the human immunodeficiency virus type 1 nucleocapsid protein facilitate efficient minus- and plus-strand transfer. *J. Virol.* 74:8980–8988.
24. Williams, M. C., I. Rouzina, J. R. Wenner, R. J. Gorelick, K. Musier-Forsyth, and V. A. Bloomfield. 2001. Mechanism for nucleic acid chaperone activity of HIV-1 nucleocapsid protein revealed by single molecule stretching. *Proc. Natl. Acad. Sci. USA.* 98:6121–6126.
25. Bernacchi, S., S. Stoylov, E. Piemont, D. Ficheux, B. P. Roques, J. L. Darlix, and Y. Mely. 2002. HIV-1 nucleocapsid protein activates transient melting of least stable parts of the secondary structure of TAR and its complementary sequence. *J. Mol. Biol.* 317:385–399.
26. Heath, M. J., S. S. Derebail, R. J. Gorelick, and J. J. DeStefano. 2003. Differing roles of the N- and C-terminal zinc fingers in human immunodeficiency virus nucleocapsid protein-enhanced nucleic acid annealing. *J. Biol. Chem.* 278:30755–30763.
27. Beltz, H., C. Clauss, E. Piemont, D. Ficheux, R. J. Gorelick, B. Roques, C. Gabus, J. L. Darlix, H. de Rocquigny, and Y. Mely. 2005. Structural determinants of HIV-1 nucleocapsid protein for cTAR DNA binding and destabilization, and correlation with inhibition of self-primed DNA synthesis. *J. Mol. Biol.* 348:1113–1126.
28. Tummino, P. J., J. D. Scholten, P. J. Harvey, T. P. Holler, L. Maloney, R. Gogliotti, J. Domagala, and D. Hupe. 1996. The in vitro ejection of zinc from human immunodeficiency virus (HIV) type 1 nucleocapsid protein by disulfide benzamides with cellular anti-HIV activity. *Proc. Natl. Acad. Sci. USA.* 93:969–973.
29. Huang, M., A. Maynard, J. A. Turpin, L. Graham, G. M. Janini, D. G. Covell, and W. G. Rice. 1998. Anti-HIV agents that selectively target retroviral nucleocapsid protein zinc fingers without affecting cellular zinc finger proteins. *J. Med. Chem.* 41:1371–1381.
30. Bombarda, E., B. P. Roques, Y. Mely, and E. Grell. 2005. Mechanism of zinc coordination by point-mutated structures of the distal CCHC binding motif of the HIV-1 NCp7 protein. *Biochemistry.* 44:7315–7325.
31. Bombarda, E., H. Cherradi, N. Morellet, B. P. Roques, and Y. Mely. 2002. Zn^{2+} binding properties of single-point mutants of the C-terminal zinc finger of the HIV-1 nucleocapsid protein: evidence of a critical role of cysteine 49 in Zn^{2+} dissociation. *Biochemistry.* 41:4312–4320.
32. de Rocquigny, H., D. Ficheux, C. Gabus, M. C. Fournie-Zaluski, J. L. Darlix, and B. P. Roques. 1991. First large scale chemical synthesis of the 72 amino acid HIV-1 nucleocapsid protein NCp7 in an active form. *Biochem. Biophys. Res. Commun.* 180:1010–1018.
33. Riddles, P. W., R. L. Blakeley, and B. Zerner. 1983. Reassessment of Ellman's reagent. *Methods Enzymol.* 91:49–60.
34. Buet, P., E. Lewitzki, E. Grell, A. M. Albrecht-Gary, K. J. Wannowius, F. Mass, H. Elias, A. A. Mundt, and Y. Dupont. 2001. Concentration jump experiments for the precise determination of rate constants of reverse reactions in the millisecond time range. *Anal. Chem.* 73:857–863.
35. Steinfeld, J. I., J. S. Francisco, and W. L. Hase. 1999. Chemical Kinetics and Dynamics. Prentice Hall, Upper Saddle River, NJ.
36. Fuoss, R. M. 1958. Ionic association. III. The equilibrium between ion pairs and free ions. *J. Am. Chem. Soc.* 80:5059–5061.
37. South, T. L., P. R. Blake, D. R. Hare, and M. F. Summers. 1991. C-terminal retroviral-type zinc finger domain from the HIV-1 nucleocapsid protein is structurally similar to the N-terminal zinc finger domain. *Biochemistry.* 30:6342–6349.
38. Stote, R. H., E. Kellenberger, H. Muller, E. Bombarda, B. P. Roques, B. Kieffer, and Y. Mely. 2004. Structure of the $His^{44} \rightarrow Ala$ single point mutant of the distal finger motif of HIV-1 nucleocapsid protein: a combined NMR, molecular dynamics simulation, and fluorescence study. *Biochemistry.* 43:7687–7697.
39. Buchsbaum, J. C., and J. M. Berg. 2000. Kinetics of metal binding by a zinc finger peptide. *Inorg. Chim. Acta.* 297:217–219.